Physica Scripta (2011) T145,014083, pp. 1-9
DOI: http://dx.doi.org/10.1088/0031-8949/2011/T145/014083

Effects of heat treatment conditions on the microstructure and impact properties of EUROFER 97 ODS steel

S F Di Martino[1], R G Faulkner[1], N B Riddle[1], M A Monge[2] and A Munoz[2]

[1] Department of Materials, Loughborough University, Leicestershire LE11 3TU, UK

[2] Departamento de Física, Universidad Carlos III de Madrid, 28911 Leganés, Madrid, Spain

E-mail: S.F.Di-Martino@lboro.ac.uk

Abstract

Probably the most important range of materials to consider for the blanket material in the tokamak design for fusion reactors such as ITER and DEMO is the high alloy Fe9Cr oxide dispersion strengthened (ODS) ferritic steels. These steels possess exceptional thermal conductivity and low thermal expansion while being strongly resistant to void swelling. Their main drawback is the high ductile-to-brittle transition temperature (DBTT), particularly in the ODS versions of the material. This paper describes attempts that are being made to reduce this DBTT in as yet unirradiated materials by a novel heat treatment procedure. The principle behind this approach is that low DBTT in the unirradiated materials will lead to relatively low DBTT even in He-containing material that has been irradiated with fusion blanket-type irradiations. New batches of high alloy Fe9Cr ODS (EUROFER) ferritic steel have been produced by a powder metallurgical route, and relatively homogeneous material has been produced by a hot isostatic pressing procedure. Mini-Charpy test specimens were made from materials that had been subjected to a matrix of heat treatments designed to show up variations in solution treatment (ST) temperature, cooling rate from the ST temperature and tempering treatment. The initial DBTT was in the range 150–200 °C. Extremely interesting results have been obtained. DBTT downward shifts of up to 200 °C have been observed by using a high 1300 °C ST temperature and a low cooling rate. The paper goes on to describe the microstructure of this material, and discusses the possible microstructural factors needed to produce these very high DBTT downward shifts. Low dissolved carbon and higher proportions of low-angle grain boundaries seem to provide the key to the understanding of the alloy behaviour.

1. Introduction

Nuclear fusion is an energy source of the future that is currently facing many material challenges. One of the most pressing is the requirement of a structural first-wall material, which must withstand high levels of neutron irradiation while maintaining sufficient mechanical properties. The most critical mechanical property requirement is of a ductile-to-brittle transition temperature (DBTT) low enough to effectively counteract the expected increase from the high levels expected from fusion neutron irradiation embrittlement.

High-chromium ferritic and ferritic martensitic steels are currently the leading candidate materials for the next fusion device to be built, ITER. Given the high irradiation dose that will be experienced by the first wall, widely used 9Cr1Mo structural steels cannot be used, due to their containing elements that have a low decay rate. This would lead to a long-term unacceptably high radioactivity level in the material, which is why research into new steels, given 'reduced activation' status not containing low decay rate elements, has been undertaken.

In Europe, the reduced activation material under development is the ferritic martensitic steel called EUROFER 97. The oxide dispersion strengthened (ODS) variant that is the focus of this study, called EUROFER ODS, contains a dispersion of yttrium oxide (0.3 wt.%). The sub-micron size of

Table 1. The heat treatment parameters investigated (FC = furnace cooling; AC = air cooling; WC = water quench).

Variables	Temperature (°C)	Time (h)	Cooling rate
Solution treatment	980	1	FC/AC/WC
	1050	1	FC/AC/WC
	1150	1	FC/AC/WC
	1300	1	FC/AC/WC
Tempering	750	1	AC

the yttria particles offers additional high-temperature strength and creep resistance through a dispersion-strengthening mechanism. One substantial disadvantage of EUROFER 97 ODS is that it has a very high DBTT.

The mechanical and physical properties and the effect of heat treatments on EUROFER variants have been widely studied [1–3]. The aim of this study is to take a combined approach, looking at the effect of solution treatment (ST) temperature and cooling rate on both the microstructure and DBTT.

The standard heat treatment for EUROFER 97 is a normalization treatment between 1050 and 1150 °C for 0.5–1 h, followed by tempering at 750 °C for 2 h [4–6]. In the present study, a range of ST temperatures between 980 and 1300 °C was investigated. These temperatures were chosen to detect the influence of heat treatment on the grain size, carbide distribution and composition and grain boundary (GB) character. This information is then used to indicate which heat treatment parameters and microstructures yield the material with the most favourable DBTT properties.

2. Experimental details

2.1. EUROFER 97 ODS processing

A EUROFER 97 ingot with the composition 0.11C-9Cr-1.1W-0.4Mn-0.2V-0.12Ta (wt.%) was cast at the Chinese Academy of Science (Shenyang, China). This was gas atomized at TLS Technik (Germany).

Mechanical alloying to combine the EUROFER 97 powder with 0.3 wt.% Y_2O_3 powder was performed at Universidad Carlos III de Madrid (Spain) in a planetary mill under a hydrogen atmosphere. Mechanical alloying was carried out at 350 rpm for 50 h at a temperature of 40 °C.

The pre-alloyed powder was then canned and degassed prior to compaction. This was subsequently performed by means of hot isostatic pressing (HIP), carried out at a temperature of 1100 °C, for 2 h, under a pressure of 190 MPa. This produced six batches of consolidated EUROFER ODS alloy.

From the as-hot isostatic pressed (as-HIPed) material, 120 miniature Charpy impact specimens with dimensions 3 mm × 4 mm × 27 mm, notch depth 1 mm and notch radius 0.1 mm were machined. The specimens were then given heat treatments in two stages: an ST followed by a cooling to room temperature and a subsequent tempering heat treatment. The variables for all heat treatments are listed in table 1.

All the heat treatments were applied at Loughborough University using a Lenton LF5* tube furnace, under a protective argon atmosphere with a flow rate of 1.5 liter s^{-1}.

Charpy V-notch impact testing was carried out at the Paul Scherrer Institute (Villigen, Switzerland) using an impact testing machine modified for use with sub-size specimens, with an atmospherically controlled chamber and an instrumented displacement sensor.

The specimens were held at the desired test temperature for 15 min using liquid nitrogen and electric heating element, with a precision of 0.1 °C. Once this hold period had elapsed, the specimen was loaded into the test position with a pneumatic rod, to allow minimal temperature deviation.

For each specimen, the Charpy impact testing machine recorded both a measured impact energy using the energy of the pendulum post-impact and a calculated energy from the load-displacement sensor in the head of the striker. All values used in this paper shall be the calculated energy taken from the displacement sensor.

3. Results and discussion

3.1. Microstructural evolution as a function of heat treatment

The mechanical alloying (MA) stage of the initial EUROFER 97 powder and the yttria dispersion is one of the most critical factors influencing the final properties of the compacted alloy [7, 8]. One of the main disadvantages of the MA route is the difficulty in reproducing the microstructure consistently. In fact, the steps involved in the alloy production (i.e. sieving, mixing, MA, degassing and HIP) make a tight control of all the variables influencing the as-HIPed microstructure (e.g. porosity, contamination, uniformity of dispersion and uniformity of grain size) a difficult task. It can be, therefore, at times difficult to draw definitive conclusions regarding process optimization, since the microstructure of the samples analysed can differ from batch to batch due to different factors.

In the present study MA and compaction were successfully conducted, although in some samples (see section 3.4) some residual porosity was encountered. In this study, porosity has proven to be a random occurrence since it has been encountered in some of the samples mechanically tested, but not in those analysed by means of microscopy. This is due to the difficulty in consistently obtaining a pore-free material in all the HIPed batches.

Taking into account the above comments, it is considered that the similarity of the procedures used to produce the mini-Charpy specimens from the elemental powders was sufficiently consistent to make the comparative DBTT results significant. It is accepted that the absolute values of Charpy energy measured may not be exactly consistent with those obtained from samples made in other production facilities.

The contamination of the powder as a function of milling parameters is shown in table 2.

The as-HIPed microstructure is martensitic with a non-uniform precipitate distribution. Large ferrite grains ($>2\,\mu$m) are present in the microstructure.

Scanning electron microscopy (SEM) analysis of the heat-treated samples suggests that, irrespective of the ST temperature, the microstructure appears to be similar in all cases, the main features being the following.

1. Fine-grained ferritic matrix (sub-micron size).
2. Fine and uniform carbide population, decorating GBs and, to a lesser extent, precipitated intragranularly (50–300 nm).

Table 2. Powder contamination during MA.

Material	Milling time (h)	Oxygen content (%)	Carbon content (%)	Nitrogen content (%)
EUROFER 97 as atomized	x	0.0277	0.1	0.034
EUROFER 97 ODS milled in H_2	50	0.131	0.133	0.02
EUROFER 97 ODS milled in H_2	60	0.143	0.136	0.016

3. Fine and uniform yttria dispersion (10–30 nm).
4. Randomly distributed regions of large ferritic grains retained after the heat treatments.

When the ST is followed by a high cooling rate (i.e. air cooling or water quench), a large amount of precipitates decorates the GB regions. On the other hand, slow cooling (i.e. furnace cooling) causes a considerable amount of precipitation to take place intragranularly. Finally, at the highest ST temperature and lowest cooling rate, the precipitates appear to be generally higher in density and coarser (see figures 1(a) and (b)).

Tunnelling electron microscopy (TEM) analysis of the normalized and tempered samples confirms the microstructural findings provided by SEM analysis, showing a ferritic matrix with low dislocation density, carbides precipitated at GBs and within the grains, and the yttria dispersion in all the heat-treated samples. The elemental analysis suggests that the coarser round precipitates are $M_{23}C_6$ (containing tungsten), while the needle-like precipitates are of the MX type (containing vanadium). No tantalum-containing carbides have been identified, possibly indicating segregation of this element at the oxide particles. Segregation of Ti to similar oxide particles in Ti-containing versions of high-Cr ODS materials (YWT alloys) has been observed [9]. The yttria dispersion presents the same morphology as observed in the SEM analysis, confirming average dimension and distribution. These findings are shown in figures 2(a)–(d).

The micro-hardness was also measured (figure 3). This shows that a lower cooling rate produces a softer material. Also, there is a slight reduction in hardness with increasing ST temperature.

Electron backscattered diffraction (EBSD) analysis has been performed on all the processed samples to obtain statistically meaningful information about the effects of the heat treatments on the grain size and the GB character. The EBSD results confirmed t hat, i rrespective o f t he ST and cooling rate, the microstructure appears similar in all the samples analysed. There is no evident texture and the grain structure is isotropic. There is no clear effect of ST temperature on the average grain size (see figure 4). The grain growth is prevented even at the highest ST temperature, within the ST time of 1 h. This is a clear sign that the GB pinning ability of the yttria particles is active. Finally, the phase map in figure 5 shows that the nature of the larger grains is δ-ferrite.

3.2. GB character analysis

The GB character distribution analysis (figure 6) indicates that the fraction of high-angle grain boundaries (HAGBs) remains strongly predominant (between 60 and 80% of the total boundary length), except for the highest ST temperature and lowest cooling rate sample (i.e. labelled as 1300FC).

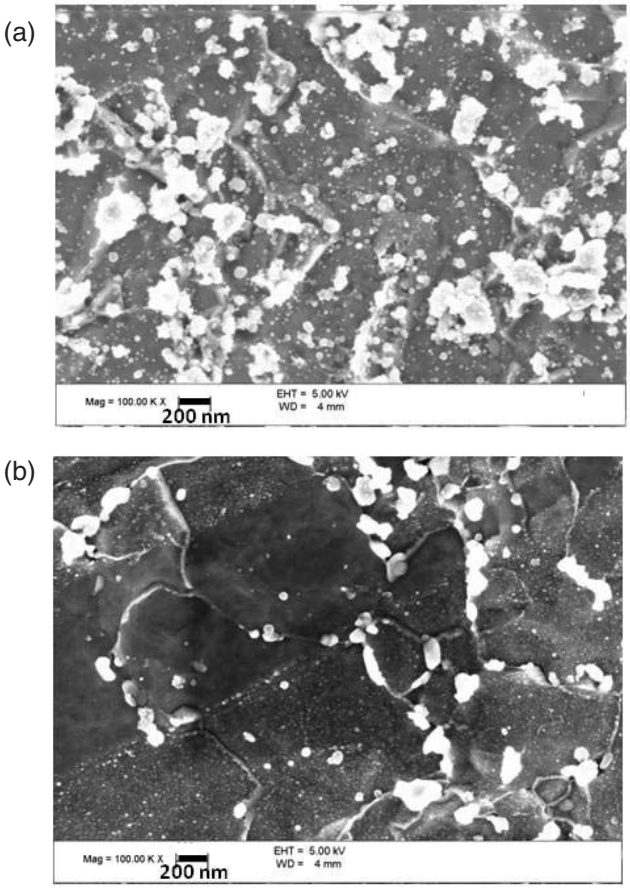

Figure 1. (a) EUROFER 97 ODS normalized at 1300 °C for 1 h, furnace cooled and tempered at 750 °C for 1 h; (b) EUROFER 97 ODS normalized at 1150 °C for 1 h, air cooled and tempered at 750 °C for 1 h.

In figure 6, the criterion to distinguish between high, low and medium angle GBs is shown on the legend. Special boundaries are not considered in this plot.

Figure 6 shows that at the ST temperature of 1300 °C, followed by furnace cooling, the fraction of LAGBs increases considerably.

Besides the distribution and dimensions of precipitates, the LAGB fraction represents the main microstructural distinction produced by the different heat treatments. For this reason, the evolution of the GB character in the sample 1300FC and, for comparison, in sample 1300WC has been monitored prior to the tempering heat treatments. Table 3 shows that in both cases, after the solution treatment, the fraction of LAGBs is very low. This indicates that the increase in LAGBs in sample 1300FC is probably partly due to high-temperature polygonization in an otherwise low dislocation ferritic matrix.

3.3. DBTT properties of HIPed EUROFER 97 ODS as a function of heat treatment

Mini-Charpy testing has been performed on all the heat-treated samples, thus providing information about the behaviour of the material produced as a function of the 12

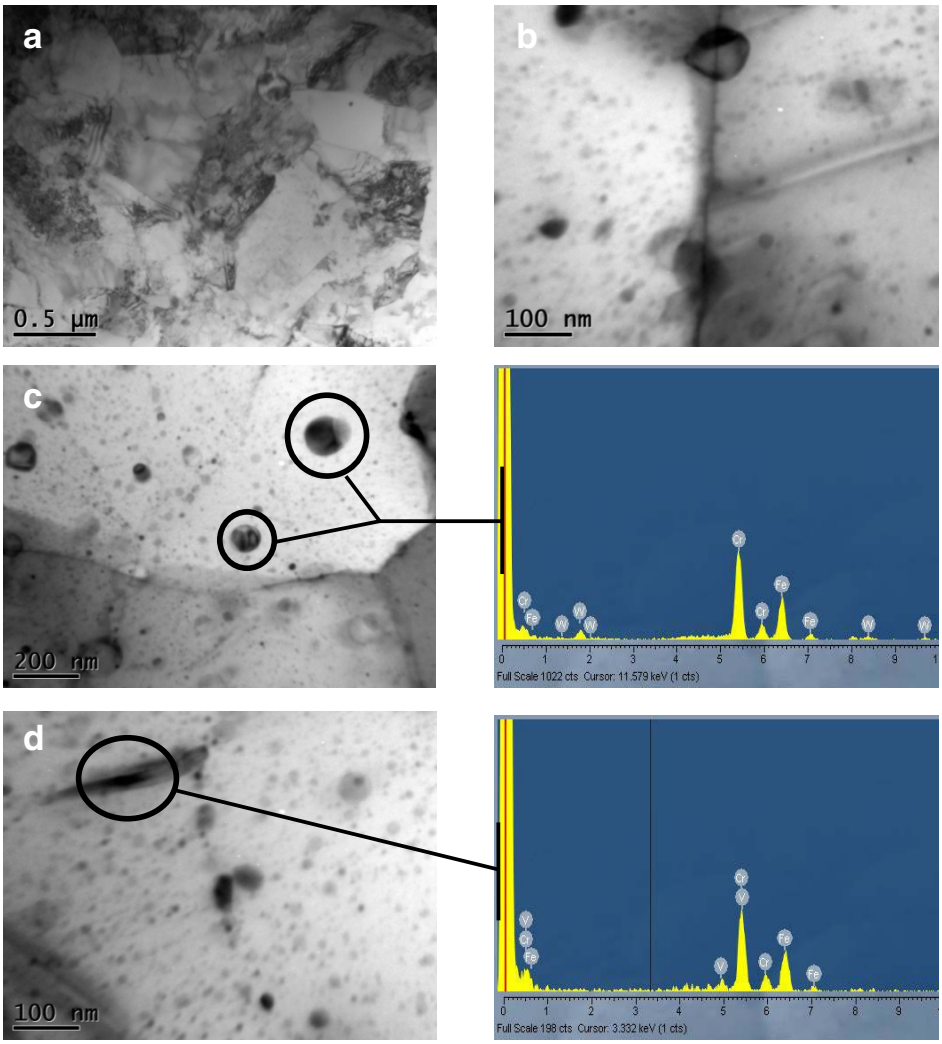

Figure 2. (a) Ferritic matrix, (b) fine yttria dispersion and precipitates at the GB and inside the grain, (c) tungsten carbides and relative EDX spectrum and (d) vanadium carbide and relative EDX spectrum.

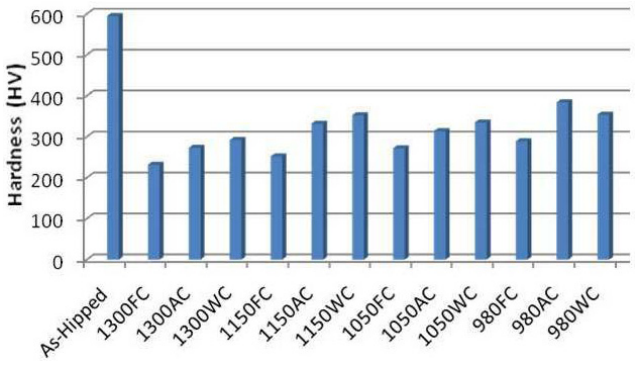

Figure 3. Micro-hardness of EUROFER 97 ODS alloy as a function of processing conditions.

heat treatment combinations tested. Figures 7(a)–(d) show the effects of cooling rate on the DBTT behaviour of the alloy for a given ST temperature. The results are summarized in table 4.

The DBTT curve of the alloy normalized at 1150 °C and water quenched could not be determined due to the large data scatter. The DBTT curve relative to the alloy normalized at 980 °C and furnace cooled does not present a clear transition temperature.

Figure 7(a) shows that the best DBTT behaviour belongs to the alloy normalized at 1300 °C and furnace cooled prior to the tempering heat treatment. The low DBTT temperature is approximately −50 °C and the upper shelf energy (USE) is approximately 5.5 J.

The alloy, normalized at 1150 °C, and furnace cooled before tempering, displays a DBTT of approximately −65 °C. However, its USE, of approximately 2 J, is still very unsatisfactory.

Figure 8 shows the difference in fracture surface between the alloy 1300FC (which has the best impact behaviour) and the alloy 1150AC, tested at three different temperatures.

Below the DBTT of both alloys (i.e. at −75 °C) the fracture mode appears to be characteristic of cleavage (figure 8(a)). In the brittle regime it is apparent that the prevalent fracture mode in this material is transgranular cleavage, although the presence of a minor degree of intergranular fracture cannot be discounted.

At room temperature (figure 8(b)), the alloy normalized at 1150 °C and air cooled (material labelled as 1150AC) shows cleavage fracture, while the alloy normalized at 1300 °C and furnace cooled (material labelled as 1300FC) shows a mixed type of fracture (predominantly ductile).

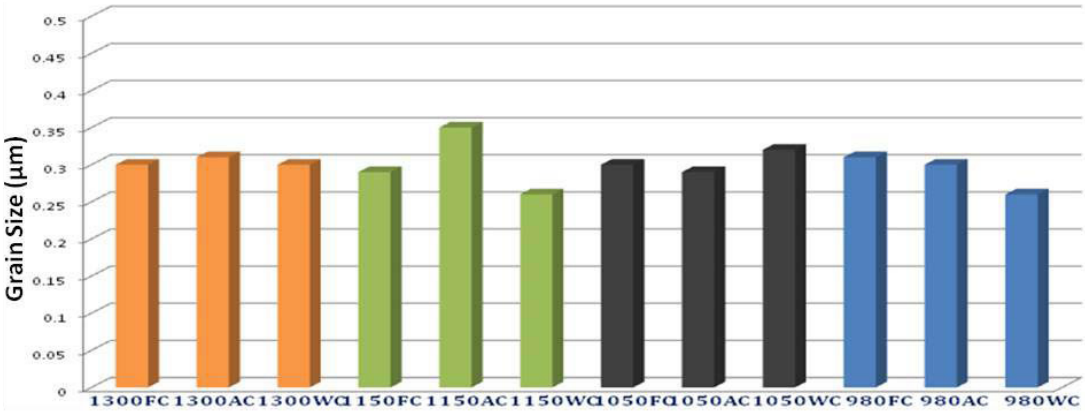

Figure 4. Average grain size of EUROFER 97 ODS, measured by means of EBSD analysis, as a function of ST temperature and cooling rate; all the samples underwent tempering treatment at 750 °C for 1 h after the ST stage.

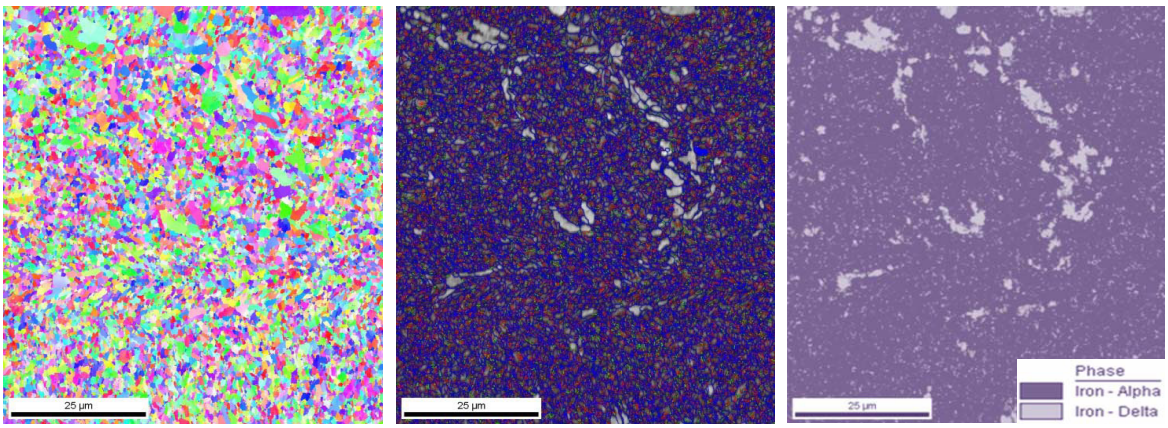

Figure 5. Inverse pole figure orientation map (left), GB character map (centre) and phase map (right) for alloy EUROFER 97 ODS normalized at 1300 °C for 1 h, water quenched.

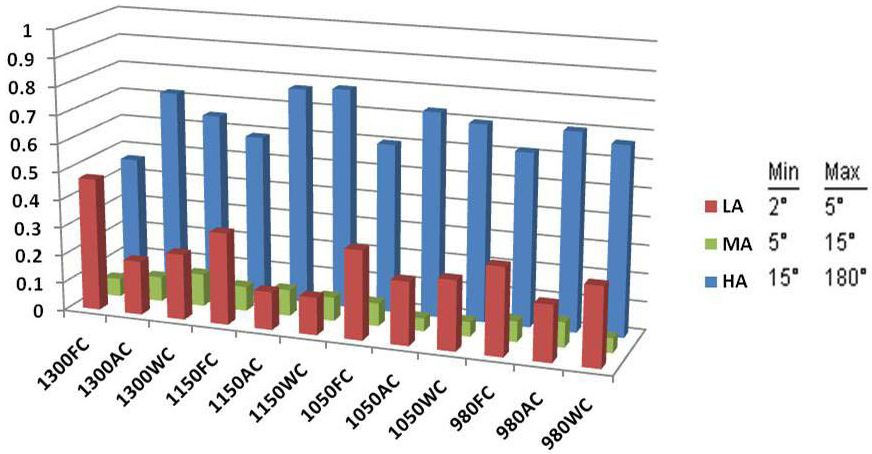

Figure 6. GB character distribution analysis for the 12 HT combinations investigated (LA = low-angle boundary; MA = medium-angle boundary; HA = high-angle boundary).

Finally, at high temperature (i.e. 120 °C) the alloy 1150AC still shows a mixed type of fracture, while the alloy 1300FC shows micro-dimples typical of ductile fracture. The larger cavities (∼5 μm diameter) are pores present in this particular batch of samples. Porosity is expected to be detrimental to the DBTT properties of the alloy.

A clear correlation between the ST temperature, cooling rate and DBTT can be identified. A lower cooling rate produces a material that shows the highest and the lowest DBTT. Also, the highest ST temperature (i.e. 1300 °C) produces the best material with the lowest DBTT and the highest USE. The shift in DBTT between the higher ST temperatures (i.e. 1300 °C) and the lower ones is very large, reaching a 250 °C difference between alloys 1300FC and 1050WC.

The following arguments are made in favour of the superior properties of the specimen 1300FC. The microstructural analysis strongly points to the following

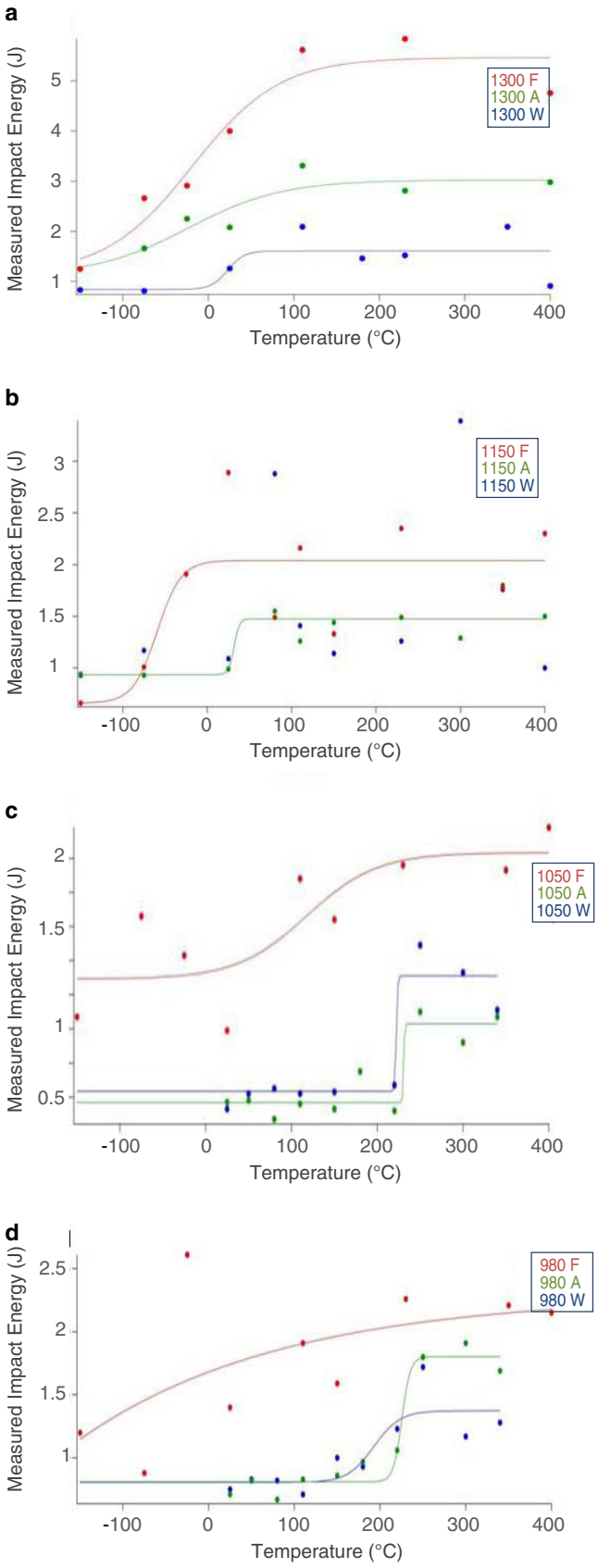

Figure 7. DBTT curves as a function of cooling rate for (a) EUROFER 97 ODS alloy normalized at 1300 °C for 1 h and tempered at 750 °C for 1 h; (b) EUROFER 97 ODS alloy normalized at 1150 °C for 1 h and tempered at 750 °C for 1 h; (c) EUROFER 97 ODS alloy normalized at 1050 °C for 1 h and tempered at 750 °C for 1 h; (d) EUROFER 97 ODS alloy normalized at 980 °C for 1 h and tempered at 750 °C for 1 h.

Table 3. Low-angle GB fraction before and after tempering for EUROFER 97 ODS alloy, normalized at 1300 °C, as a function of cooling rate.

Material	LAGB fraction before tempering (%)	LAGB fraction after tempering (%)
1300FC	12	44
1300WC	18	22

Table 4. DBTT temperature (a) and USE (b) for EUROFER 97 ODS as a function of cooling rate and ST temperature.

Cooling rate	ST temperature			
	980 °C	1050 °C	1150 °C	1300 °C
	DBTT (°C)			
Furnace cooling (FC)	–	130	−65	−50
Air cooling (AC)	180	220	40	−40
Water quench (WC)	220	225	–	20
	USE (J)			
Furnace cooling (FC)	–	2	2	5.5
Air cooling (AC)	1.8	1.3	1.5	2.8
Water quench (WC)	1.4	1	–	1.5

microstructural features:

1. lower hardness;
2. a larger amount of precipitates;
3. a larger fraction of LAGBs;
4. a lower dislocation density.

The pinning ability of yttria allows the retention of fine grain size even at the high ST temperature of 1300 °C and provides a microstructural characteristic that helps reduce the DBTT. At the same time, at such a high temperature the uniform dissolution of all elements present in the base powder can be more effectively achieved.

The low hardness represents one of the keys to the improved DBTT properties of the 1300FC material. As a result of the very high ST temperature and very slow cooling, a softer matrix is available, and assuming that the cleavage fracture stress is stable, a net DBTT reduction results (see figure 9). Thermodynamic calculations are currently being performed in order to study possible alterations in the carbon solubility at a very high ST temperature, which could in turn affect the type of transformations taking place upon cooling (MTDATA).

The increase in USE in the 1300ST samples is the typical behaviour of a low-carbon-content microstructure (see figure 10 for a comparison of low- and high-carbon-content steels).

The other key to explain the improved DBTT properties of the 1300FC samples is the high fraction of LAGBs observed. This can be used to explain a reduction in DBTT. A recent cleavage fracture stress analysis [10] defined the cleavage fracture stress σ_F:

$$\sigma_F = \sqrt{\frac{EG}{\pi d}}, \tag{1}$$

where E is Young's modulus, G is the work of fracture ($= K_{Ic}^2/E$), K_{Ic} is the plain strain fracture toughness and d is a distance parameter, usually the grain size.

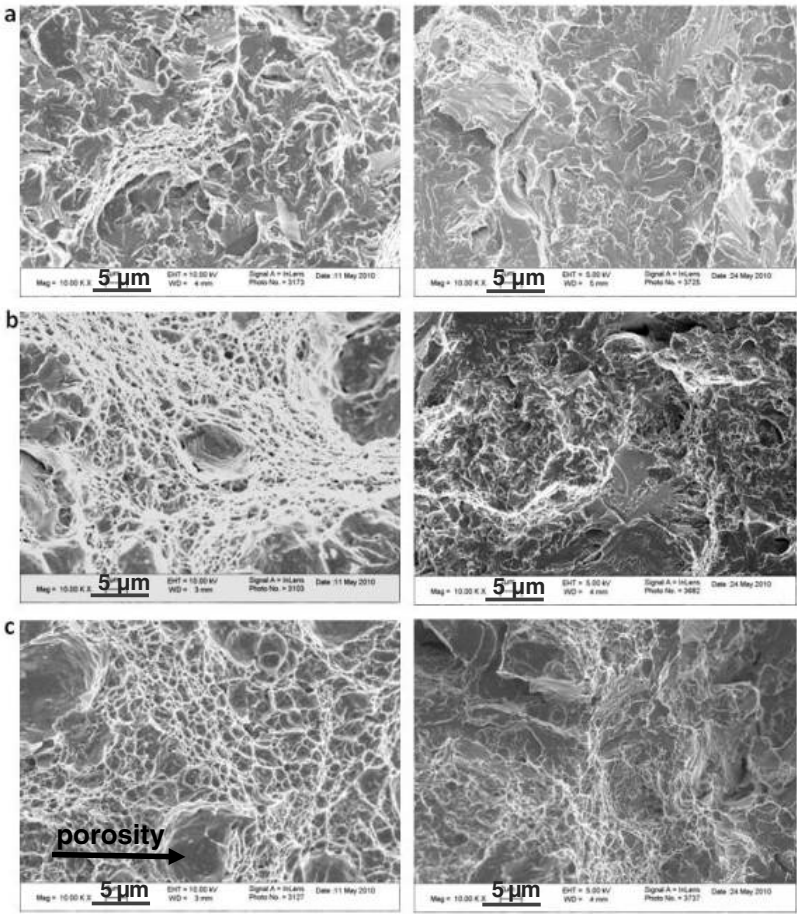

Figure 8. Comparison between fracture surfaces of EUROFER 97 ODS 1300FC (left images) and 1150AC (right images): (a) samples tested at −75 °C; (b) samples tested at room temperature; (c) samples tested at 120 °C.

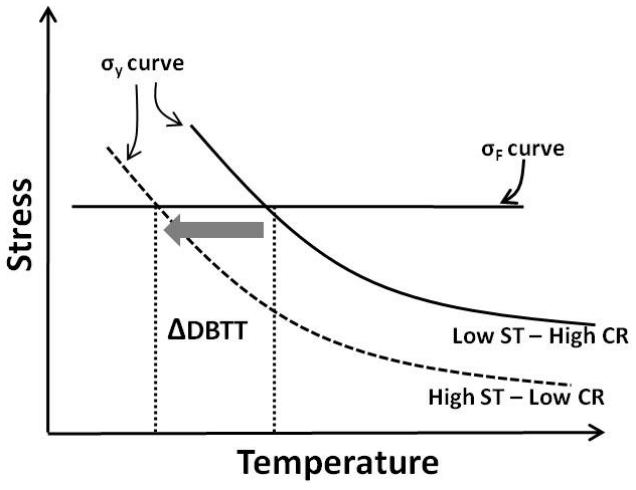

Figure 9. Schematic representation of the DBTT reduction caused by increasing ST temperature and decreasing cooling rate (CR) prior to tempering [12, 13].

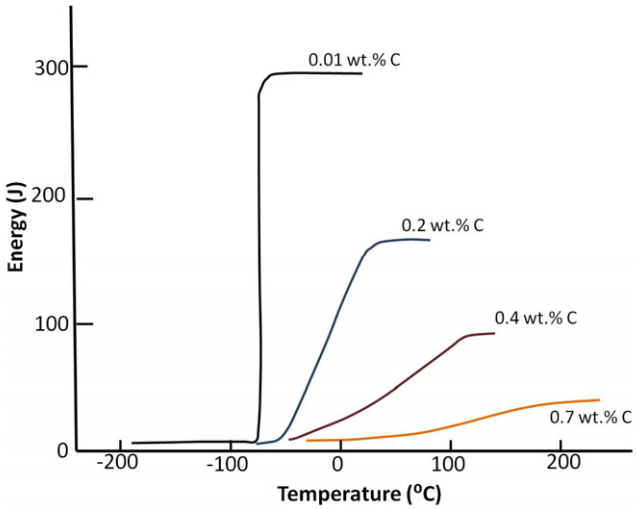

Figure 10. Effect of carbon content on the impact energy temperature plot for annealed steels [11].

The work of fracture, G, for a cleavage crack is controlled by

- surface energy,
- plastic deformation ahead of the propagating crack, and
- barriers to crack propagation, such as GBs and precipitates.

Recent studies [10] have shown that the GB barrier energy is strongly related to

- GB character,
- degree of precipitation,
- segregation, and
- grain size.

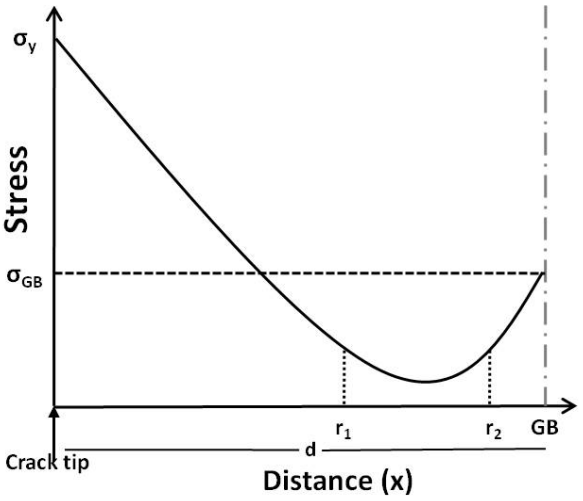

Figure 11. Schematic representation of the stress profile ahead of the crack tip. The stress rises in correspondence to an obstacle (such as a GB). The character of the GB, degree of precipitation and segregation influence the extent of increase in the GB cleavage stress, σ_{GB}.

The cleavage crack propagation stress, per unit length of crack, x_1, is a function of distance ahead of the crack. The energy absorbed by the crack is

$$G = \int_0^x \frac{x}{d}\left(\frac{\sigma_y}{2r_1} + \frac{\sigma_{GB}}{2(d-r_2)}\right) dx, \qquad (2)$$

where d is the grain size; σ_y is the yield stress; σ_{GB} is the stress required to fracture the GB (depending on GB character and precipitation density); and r_1 and r_2 are material constants indicating the distance from the crack tip, r_1, and from obstacles such as the GB, r_2, for the stress concentration to reduce to zero ($\sim$4 μm in steels). This is schematically shown in figure 11.

The GB character generally leads to a reduced energy for the low angle boundaries. The degree of precipitation on LAGBs is usually very low, and hence in the case discussed here, we have a higher than normal proportion of LAGBs, which are decorated with fewer precipitates than normal. The cleavage fracture paths are easier along the high-energy precipitate–matrix interfaces. Since there are fewer GB precipitates in the 1300FC material the cleavage across the GBs becomes more difficult a nd G increases. This results in reduced DBTT, assuming that the matrix fracture strength temperature dependence remains the same (see figure 12).

4. Conclusions

The production of EUROFER 97 ODS, containing yttria particles via MA and HIP, has been successfully carried out.

The microstructures obtained show very fine grains (sub-micron size) although a few areas have larger δ-ferrite grains ($>2\,\mu$m); the yttria appears as a fine dispersion of particles with sizes ranging between 10 and 30 nm; the carbide population appears to be uniform and consists mainly of $M_{23}C_6$ and, to a lesser extent, MC; the precipitates are mostly found at GBs. No tantalum carbides have been identified to

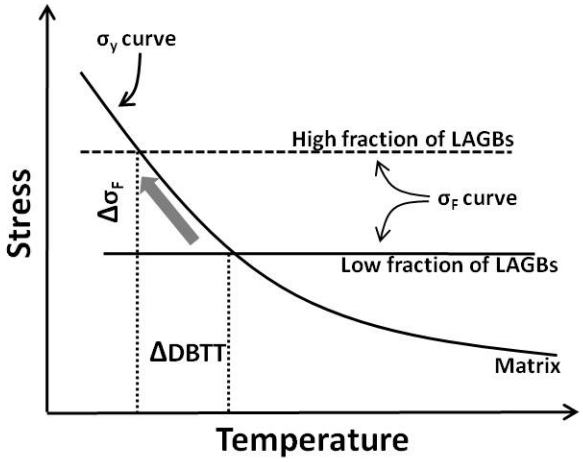

Figure 12. Schematic representation of the DBTT shift caused by an increase in LAGB fraction in the microstructure.

date, possibly indicating segregation of this element at the yttria particles. The average grain size of the samples remains within the same range at all ST temperatures, indicating that GB pinning by the yttria particles is active.

The grain orientation distribution remains similar at all ST temperatures, except that the fraction of LAGBs increases at the highest ST temperature and lowest cooling rate. The hardness of the tempered material is also lower in the highest ST and lowest cooling rate case.

Important conclusions can be drawn: increasing the ST temperature and decreasing the cooling rate (1300FC) has proven to be very beneficial to the DBTT properties of the alloy, producing downward shifts of 250 °C.

In the lower shelf regime, the most evident brittle fracture mode identified is transgranular cleavage.

The suggested heat treatment for the very low DBTT is ST at 1300 °C for 1 h, followed by furnace cooling and tempering at 750 °C for 1 h—this alloy displayed a USE of 5.5 J and a DBTT of −50 °C.

References

[1] Lässer R, Baluc N, Boutard J-L, Diegele E, Dudarev S, Gasparotto M, Möslang A, Pippan R, Riccardi B and van der Schaaf B 2007 Structural materials for DEMO: the EU development, strategy, testing and modelling *Fusion Eng. Des.* **82** 511–20

[2] Lu Z, Faulkner R G, Riddle N, Di Martino F and Yang K 2009 Effect of heat treatment on microstructure and hardness of EUROFER 97, EUROFER ODS and T92 steels *J. Nucl. Mater.* **386–388** 445–8

[3] Ramar A, Oksiuta Z, Baluc N and Schäublin R 2007 Effect of mechanical alloying on the mechanical and microstructural properties of ODS EUROFER 97 *Fusion Eng. Des.* **82** 2543–9

[4] McClintock D A, Sokolov M A, Hoelzer D T and Nanstad R K 2009 Mechanical properties of irradiated ODS-EUROFER and nanocluster strengthened 12YWT *J. Nucl. Mater.* **392** 353–9

[5] Yamamotoa M, Ukaia S, Hayashia S, Kaitob T and Ohtsukab S 2010 Formation of residual ferrite in 9Cr-ODS ferritic steels *Mater. Sci. Eng.* A **527** 4418–23

[6] Chaouadi R, Coen G, Lucon E and Massaut V 2010 Crack resistance behavior of ODS and standard 9%Cr-containing steels at high temperature *J. Nucl. Mater.* **403** 15–8

[7] Barrie M 2003 Fabrication of steels for advanced power plant *Mitsui Babcock Energy Ltd Report* R226/DTI/Pub URN 02/1508
[8] Sikka V K, Ward C T and Thomas K C 1981 Production, fabrication, properties and applications of ferritic steels for high temperature applications *ASM Int. Conf. (Warren, PA, October 1981)* pp 65–84
[9] Aloinger M J, Odette G R and Hoelzer D T 2009 On the role of alloy composition and processing parameters in nanocluster formation and dispersion strengthening in nanostructured ferritic alloys *Acta Mater.* **57** 392–406
[10] Faulkner R G and Riddle N 2011 Control of ductile to brittle transition temperature in ferritic pressure vessel steel *Mater. Sci. Technol.* **27** 300–4
[11] Rinebolt J A 1951 Effect of alloying elements on notch toughness of pearlitic steels *Trans. ASM* **43** 1175
[12] Yin Y and Faulkner R G 2003 Simulations of precipitation in ferritic steels *Mater. Sci. Technol.* **19** 91
[13] Yin Y and Faulkner R G 2002 *Power Technology* vol 21 (Jülich: Forschungszentrum Jülich GmbH) pp 1247–56